Integrated Stress Response Signatures Drive Monocyte Dysfunction in *GBA1*- and *LRRK2*-Linked Parkinson's Disease

Authors: Daniele Mattei[1-4#], Erica Brophy[1-4#], Mikaela Rosen[1-4], Oriol Narcis Majos[1-4], Aloysius Domingo[5,6], Elena Meijia[1-4], Claudia De Sanctis[11,12], Beomjin Jang[1-4], Tarek Khashan[1-4], Mengxi Yang[7,8], Deborah Raymond[7,8], Casey Young[7,8], Jack Humphrey[1-4], Elisa Navarro[1-4,10], , Amanda Allan[1-4], Katherine Leaver[7,8], Viktoriya Katsnelson[7,8], Alexander Chung[1-4], Benjamin Muller[1-4], Matthew Swan[7,8], Vicki L. Shanker[7,8], Mariel Pullman[7,8], Adina Wise[7,8] , Roberto Ortega[7,8], Kelly Astudillo[9], Steven Frucht[9], Susan Bressman[7,8], Giulietta Riboldi[9], Laurie J. Ozelius[5,6], Rachel Saunders-Pullman[7,8], Towfique Raj[1-4,7*]

Affiliations:

[1]Department of Genetics and Genomic Sciences, Icahn School of Medicine at Mount Sinai, New York, NY, USA.

[2]Nash Family Department of Neuroscience & Friedman Brain Institute, Icahn School of Medicine at Mount Sinai, New York, NY, USA.

[3]Ronald M. Loeb Center for Alzheimer's Disease, Icahn School of Medicine at Mount Sinai, New York, NY, USA.

[4]Icahn Genomics Institute, Icahn School of Medicine at Mount Sinai, New York, NY, USA.

[5]Department of Neurology, Massachusetts General Hospital and Harvard Medical School, Boston, MA 02114, USA.

[6]Center for Genomic Medicine, Massachusetts General Hospital, Boston, MA 02114, USA.

Program in Medical and Population Genetics, Broad Institute, Cambridge, MA 02142, USA.

[7]Department of Neurology, Icahn School of Medicine at Mount Sinai and Mount Sinai Beth Israel, New York, NY, USA.

[8]Bonnie and Tom Strauss Movement Disorders Center, Icahn School of Medicine at Mount Sinai, New York, NY, USA.

[9]The Marlene and Paolo Fresco Institute for Parkinson's and Movement Disorders, Department of Neurology, NYU Langone Health, New York City, New York, USA.

[10]Neurochemistry Research Institute, Department of Biochemistry and Molecular Biology, School of Medicine, Complutense University of Madrid, 28040 Madrid, Spain.

[11]Department of Pathology, Friedman Brain Institute, Icahn School of Medicine at Mount Sinai, New York, NY, 10029, USA.

[12]Nash Family Department of Neuroscience, Department of Psychiatry, Friedman Brain Institute, Icahn School of Medicine at Mount Sinai, New York, NY, USA.

[#]Contributed Equally

***Corresponding authors:**
Towfique Raj towfique.raj@mssm.edu; Icahn School of Medicine at Mount Sinai, New York, NY, USA.

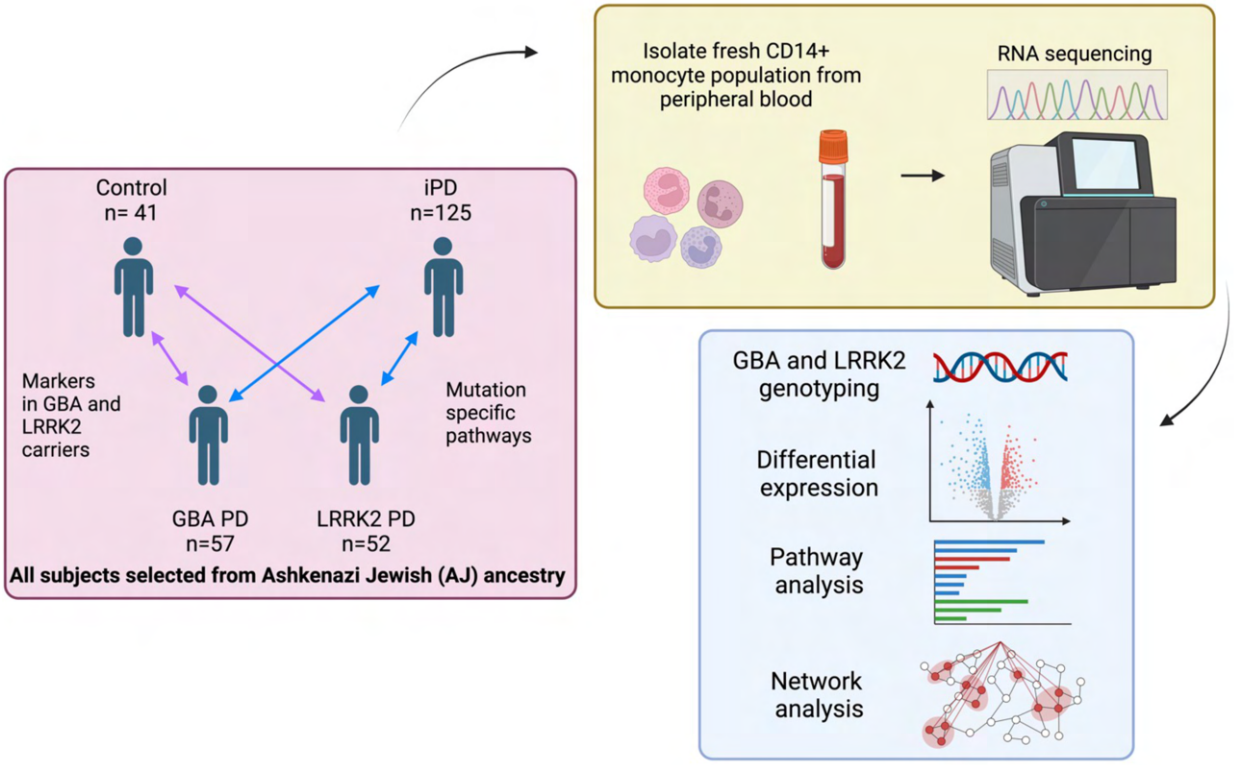

Supplementary Fig. 1 | Project design schematic representation. Schematic representation of project design and rationale for the comparison of the selected cohorts and analysis of biological samples in monocytes. Fresh CD14+ monocytes were isolated from peripheral blood within 3 hours of blood drawn from 233 donors with neurological diseases, as well as 41 unaffected subjects (controls) generating a total of 274 samples. Genome-wide genotyping was performed using DNA isolated from all donors and all subjects are from Ashkenazi Jewish European ancestry. The following analyses were performed with this dataset: (i) differential expression analysis; (ii) weighted gene co-expression analysis; (iii) gene set enrichment analysis.

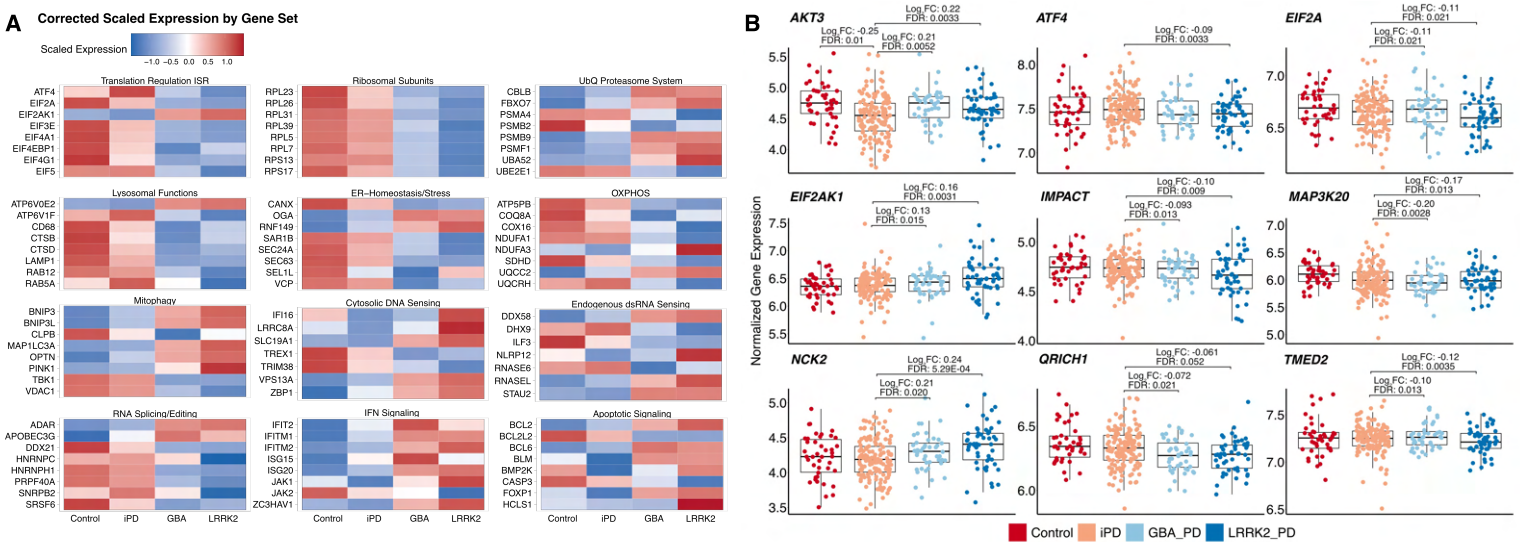

Supplementary Fig. 2 | (A) Heatmaps comparing the corrected, scaled SVA expression key genes associated with the biological processes significantly deregulated in GBA1- and LRRK2-PD monocytes relative to iPD (resolved from Fig. 1F). All displayed genes were significantly differentially expressed in either or both GBA1- and LRRK2-PD monocytes (FDR < 0.05, method = BH). Scaled expression is defined as z-score-transformed mean expression per gene, calculated by centering and standardizing SVA-corrected normalized expression. **(B)** Boxplots comparing the SVA corrected expression of core genes involved in the integrated stress response (ISR) signaling. Displayed genes are from the gene ontology term GO:0140467 (ISR signaling).

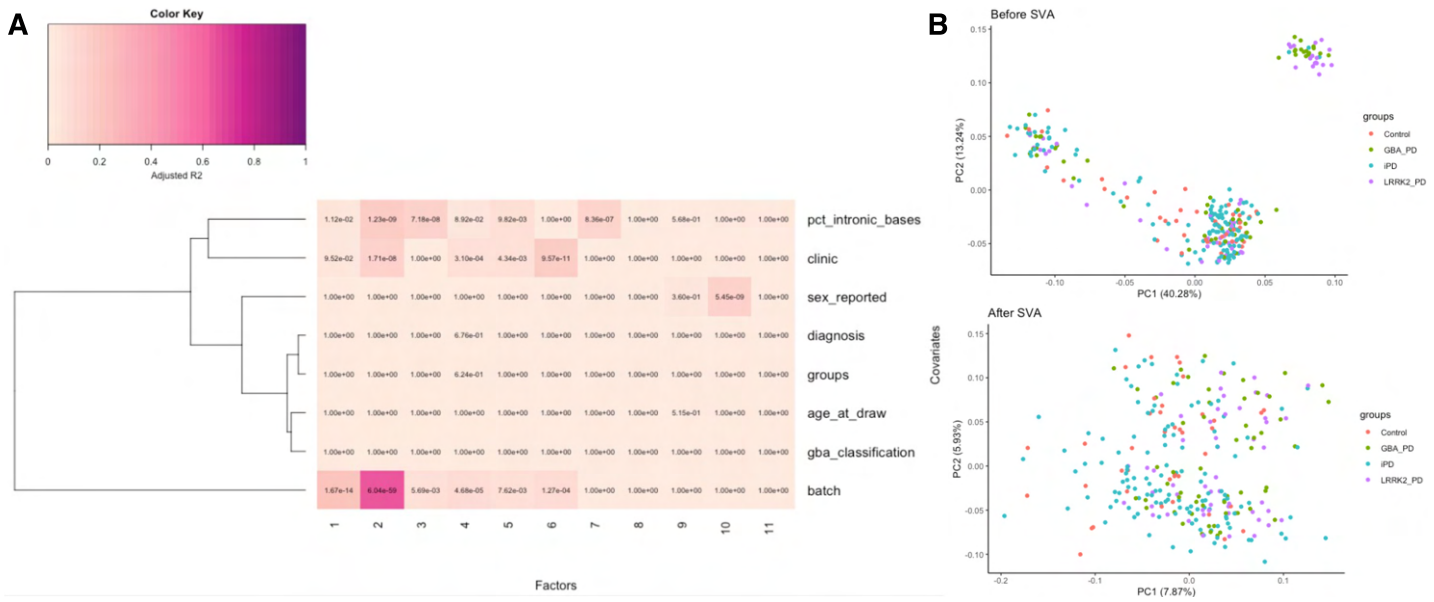

Supplementary Fig. 3 | Covariate selection and correlation with possible confounders. (A) Heatmap showing the correlation of the first 11 SVs (x-axis) and the known covariates (y-axis). (**B**) Scatter plot showing the results from the principal component (PC) analysis before and after surrogate variable analysis (SVA).

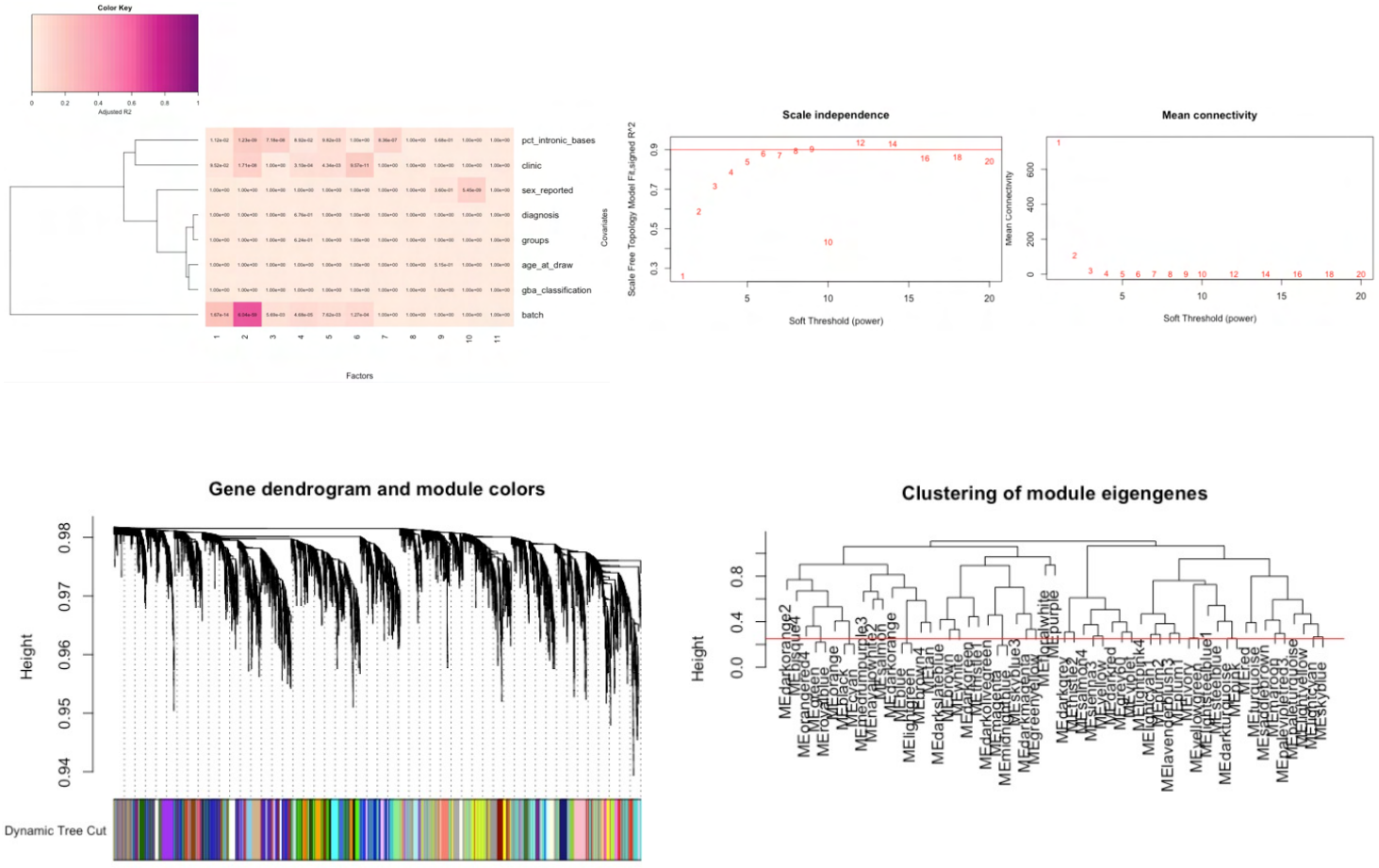

Supplementary Fig. 4 | Gene network construction in human monocytes using WGCNA. 53 unique co-expression modules were obtained using WGCNA. **(A)** Heatmap showing the correlation of the first 11 SVs (x-axis) and the known covariates (y-axis). **(B)** Right: Evaluation of network topology with different soft-thresholding powers. The y-axis represents the scale-free fit index as a function of the soft-thresholding power (x-axis). Left: The mean connectivity (y-axis) as a function of the soft-thresholding power. **(C)** Gene dendrogram using “Dynamic Tree Cut” to assign genes to different modules and modules to colors, showing before and after collapsing modules into 65 final networks. **(D)** Module eigengenes clustering dendrogram based on topological overlap. Modules below the threshold (Module Dissimilarity = 0.25) indicated by the red line were merged. These values correspond to a correlation of 0.75.

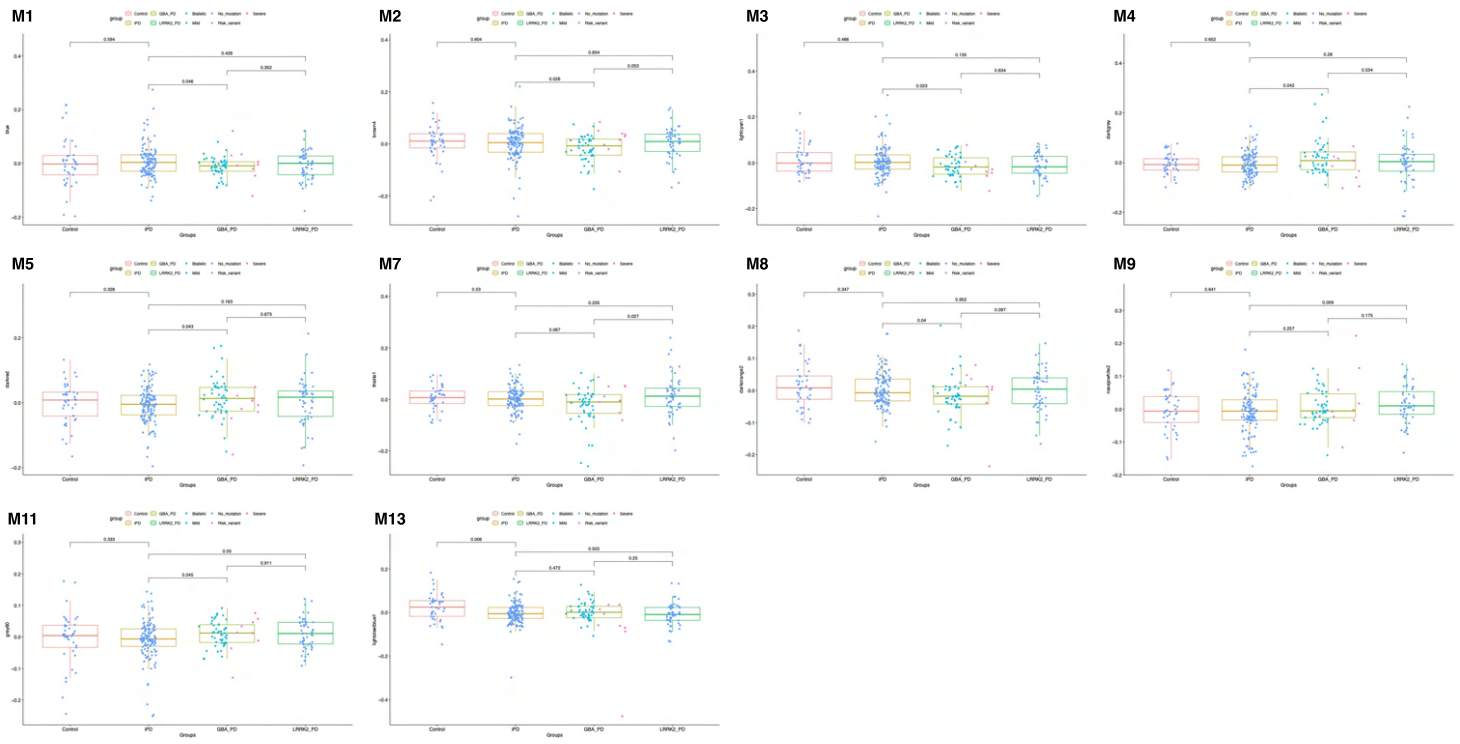

Supplementary Fig. 5 | Modules Eigengene expression comparison between groups. Boxplots show eigengene expressions for all modules except M6, M10 and M12, displayed in Fig. 3B. Boxplots indicate median, quartiles, and whiskers (1.5× IQR). Eigengene expression was compared via Wilkoxon sum-rank test, nominal p-value thresholds: *p ≤ 0.05, **p ≤ 0.01, *p ≤ 0.001.

A

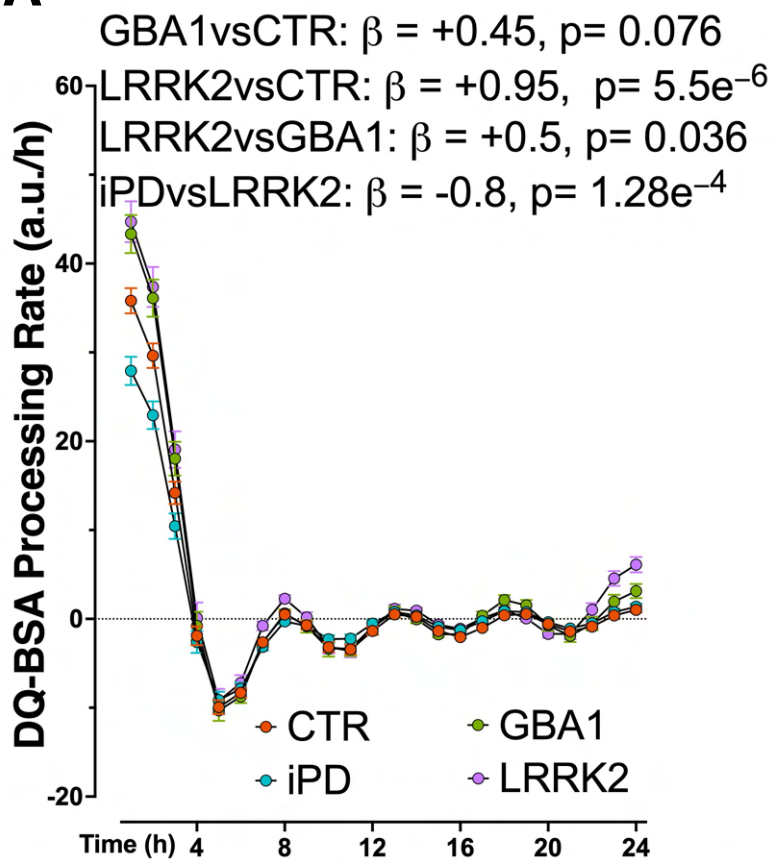

B

Wilcoxon test		
Time Point (h)	**CTR Vs.**	**FDR**
1	GBA1	0.01
1	iPD	0.001
1	LRRK2	0.013
2	GBA1	0.039
2	iPD	0.005
2	LRRK2	0.032
7	LRRK2	0.012
8	LRRK2	0.005
14	LRRK2	0.046
15	GBA1	0.014
15	iPD	0.014
15	LRRK2	0.006
16	iPD	0.016
16	LRRK2	0.036
18	GBA1	0.007
20	GBA1	0.049
20	LRRK2	0.001
22	LRRK2	0.012
23	GBA1	0.003
23	LRRK2	0.000
24	GBA1	0.001
24	LRRK2	0.000

Supplementary Fig. 6 | Altered lysosomal proteolysis rates in PD monocyte-derived macrophages (MDMs) measured with DQ-BSA. (A) Time course of covariate-adjusted DQ-BSA processing rates (a.u./h; mean ± SEM) in MDMs from controls (CTR), GBA1-PD, iPD and LRRK2-PD patients over 24 h. Rates were obtained as time-derivatives of generalized additive model (GAM)-fitted fluorescence trajectories, and compared between groups using linear mixed-effects models with donor as a random effect and age, clinic, ancestry, weeks frozen and assay date as covariates. Text reports slope (group×time) contrasts versus the indicated reference group (β, a.u./h; p). (B) Significant per-time-point differences in DQ-BSA processing rates between CTR and each PD subgroup, assessed by Wilcoxon rank-sum tests with Benjamini–Hochberg FDR correction; table lists time (h), comparison and FDR-adjusted q-values.

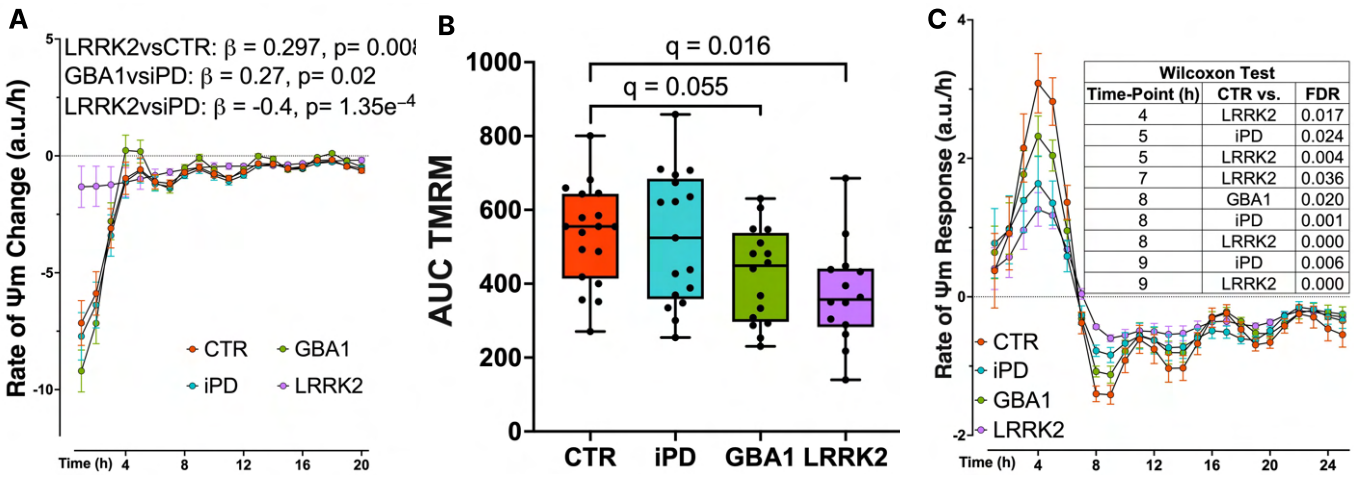

Supplementary Fig. 6 | Mitochondrial membrane potential dynamics in PD monocyte-derived macrophages. (A) Time course of covariate-adjusted rates of change in TMRM fluorescence (ΔΨm; a.u./h, mean ± SEM) in monocyte-derived macrophages (MDMs) from controls (CTR), GBA1-PD, iPD and LRRK2-PD patients at baseline. Rates were obtained as first derivatives of generalized additive model (GAM)-fitted TMRM trajectories and compared between groups with linear mixed-effects models. Text reports slope (group×time) contrasts between the indicated groups (β, a.u./h; p). **(B)** Box-and-whisker plots (min–max, line = median; each point = one donor) of subject-level TMRM area under the curve AUC at baseline. Group differences were assessed by Kruskal-Wallis test followed by pairwise Wilcoxon rank-sum tests with Benjamini–Hochberg FDR correction; q-values are shown above brackets. **(C)** Detailed time course of ΔΨm response rates (a.u./h, mean ± SEM) following 100 µM ADP, with accompanying table listing time points (h) at which CTR differed from each PD subgroup by Wilcoxon rank-sum tests (FDR-adjusted q-values).